DOI 10.1007/s11182-020-02042-2

Russian Physics Journal, Vol. 63, No. 2, June, 2020 (Russian Original No. 2, February, 2020)

LASERS AND OPTOELECTRONIC SYSTEMS

PULSED X-RAY AND CATHODOLUMINESCENCE OF PURE AND ALLOYED ZINC SELENIDE SINGLE CRYSTALS

V. I. Oleshko,[1] V. F. Tarasenko,[2] M. V. Erofeev,[2] and S. S. Vil'chinskaya[1]

UDC 537.523.9

*The paper studies the amplitude and spectral-kinetic behavior of pulsed X-ray and cathodoluminescence of non-alloyed zinc selenide (*ZnSe*) single crystals and those alloyed by gallium, tellurium and samarium. At 300 K, the spectra of pulsed cathodoluminescence of pure* ZnSe *single crystals show a 490 nm illumination at ~20 ns pulse time. Two spectral bands are observed in alloyed* ZnSe *single crystals, band edge at ~477 nm and with maximum at ~600 nm at a pulse time of ~20 ns and ~5 μs, respectively. The intensity ratio of these peaks depends on the electron-beam energy density and the geometry of spectrum measurements. X-ray luminescence spectra of the alloyed* ZnSe *single crystals show an ~600 nm illumination, the intensity of which depends on the type of impurity. The possibility of applying the pure and alloyed* ZnSe *single crystals is discussed herein for the development of amplitude-time characteristic sensors of electron beams and X-ray radiation energy ranging from tens to hundreds of kiloelectronvolts.*

Keywords: zinc selenide single crystal, luminescence spectrum.

INTRODUCTION

The radiation of various crystals is widely used to create ionizing radiation detectors [1], while electron beams are used to identify different substances by their radiation spectra [2]. Lately, the necessity emerged to detect the parameters of escaping electrons in tokamak (toroidal chamber with magnetic coils) devices [3–5]. This is due to the fact that the generation of high-energy electrons adversely affects the plasma heating and leads to the wall destruction of the working chamber. In [6, 7] it is reported about the development of detectors of escaping electrons based on the Vavilov-Cherenkov radiation in the diamond crystal. According to previous research [8, 9], the intensity of pulsed cathodoluminescence observed in the diamond crystal along with the Vavilov-Cherenkov radiation, is much higher during the e-beam irradiation process using the energy ranging from tens to hundreds of kiloelectronvolts.

As is known, the intensity of pulsed cathodoluminescence depends on the crystal type, production process and alloying [1, 8]. The intensity of the Vavilov-Cherenkov radiation depends on the electron energy and the refractive index of matter [7–9, 10–12]. During the e-beam irradiation of natural and synthetic diamonds at electron energy up to 200 keV, the pulsed cathodoluminescence is higher than the Vavilov-Cherenkov radiation [8].

Zinc selenide (ZnSe) single crystals are investigated in this work as they belong to the most promising wide-bandgap materials of the A_2B_6 type. ZnSe single crystals possess the high light output and low luminescence decay time, temperature and radiation stability of output parameters, *i.e.* remain operable up to 10^7–10^8 rad, and find wide application as ionizing radiation detectors and in manufacturing e-beam pumped semiconductor lasers [13]. The

[1]National Research Tomsk Polytechnic University, Tomsk, Russia, e-mail: oleshko@tpu.ru; svetvil@tpu.ru; [2]Institute of High Current Electronics of the Siberian Branch of the Russian Academy of Sciences, Tomsk, Russia, e-mail: VFT@loi.hcei.tsc.ru; mve@loi.hcei.tsc.ru. Translated from Izvestiya Vysshikh Uchebnykh Zavedenii, Fizika, No. 2, pp. 117–122, February, 2020. Original article submitted December 16, 2019.

radiation stability of alkali-halide crystals of the CsI(Tl) type is considerably lower; their light output lowers at ~$2 \cdot 10^3$ rad.

This work focuses on studying the amplitude and spectral-kinetic behavior of pulsed X-ray and cathodoluminescence of non-alloyed and alloyed ZnSe single crystals, that can be used for the detection of escaping electrons and attendant X-ray radiation in tokamak devices.

EXPERIMENTAL TECHNIQUES

In these experiments, ZnSe polycrystalline made by chemical vapor deposition (CVD) was used as the source for ZnSe single crystal growth. Also, ZnSe single crystals grown at the Institute of Single Crystals (Kharkiv, Ukraine) were alloyed by elements belonging to groups III and VI. The alloyed ZnSe crystals were grown using the Bridgman method, under the gas argon pressure of $2 \cdot 10^6$ Pa in the process chamber. The ZnSe specimens 8×8×2 mm in size were then subjected to the implantation of alloying elements in the concentration ranging between $5 \cdot 10^{-3}$ and $1 \cdot 10^{-2}$ vol.%. The experiments were carried out at 300 K on the unit described in our earlier research [14]. A high-current electron accelerator based on GIN-600 pulse generator was used to produce pulsed X-ray and pulsed cathodoluminescence. The maximum electron energy in the spectrum was 300 keV. The half-height pulse duration was ~12 ns, the energy density ranged from 0.01 to 0.25 J/cm^2. The X-ray pulses were obtained by the energy loss in the e-beam of about 1 J/cm^2 energy density in the copper anode and ~100 μm thick. We used two ways of recording the luminescence spectra of the ZnSe specimens, *viz*. point by point recording and light sum per pulse recording.

The point by point recording allowed the luminescence spectra to be measured with time resolution, using a pulsed optical spectrometer. The ZnSe specimens were placed at the e-beam incident angle of ~45 or 90 degrees. The specimen image was projected onto the slit of an MDR-23 monochromator with the diffraction grating consisting of 1200 grooves per millimeter, with a 1.3 nm/mm inverse linear dispersion. The amplitude and spectral-kinetic characteristics of the pulsed X-ray and pulsed cathodoluminescence were recorded by a photomultiplier tube FEU-84 operating in the 300–850 nm wavelength range and at ~7 ns transient response plus a Tektronix DPO 3034 Digital Oscilloscope 300 MHz and ~20 ns time resolution.

The light sum per pulse recording allowed the luminescence spectra to be measured without time resolution, using the AvaSpec-ULS2048CL-EVO Spectrometer (Avantes, Netherlands) with the wavelength range of 190–1100 nm and ~2 nm spectral resolution. The irradiated crystal surface was placed at an angle of ~45 or 90 degrees to the e-beam propagation. The luminescence spectra of the ZnSe specimens were registered at the ends, from the non-irradiated surface, at an angle of 45 degrees to the irradiated surface. Transmission spectra of the ZnSe specimens of different compositions were recorded in the 400–800 nm wavelength range on an SF-256 spectrophotometer.

RESULTS AND DISCUSSION

Based on our research and the analysis of works of other researchers, we found that the amplitude and spectral-kinetic behavior of pulsed X-ray and cathodoluminescence of ZnSe single crystals depended on their growth technique, irradiation intensity, the geometry of spectrum measurements, and recording methods.

The transmission spectra in Fig. 1 belong to non-alloyed ZnSe single crystals and Ga-, Te- and Sm-alloyed ZnSe crystals made by the CVD method. One can see that the absorption edge of the alloyed crystals shifts to the long-wave region relative to the fundamental absorption edge of the CVD-grown crystals. The largest shift and the lower transmission in the absorption edge are observed in the ZnSe(Ga) crystal, that indicates to the high concentration of both shallow and deep levels in the forbidden gap of the crystal.

The pulsed X-ray luminescence of the alloyed crystals (excitation energy $G \sim 10^{19}$–10^{20} cm^{-3}·s^{-1}) in Fig. 2 shows that the luminescence spectra of the specimens measured by the light sum per pulse method represent one wide band with maximum at ~600 nm and the full width at half maximum (FWHM) at ~345 meV; its intensity depends on the type of the implanted alloying element (see Table 1).

TABLE 1. Relative Intensity of Luminescence Spectra at 600 nm Wavelength in Alloyed ZnSe Single Crystals

ZnSe crystals	Intensity, a. u.
CVD-grown	0
Ga-alloyed	100
Te-alloyed	33
Sm-alloyed	23

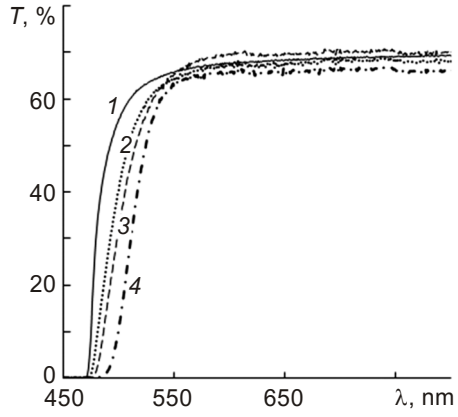

Fig. 1

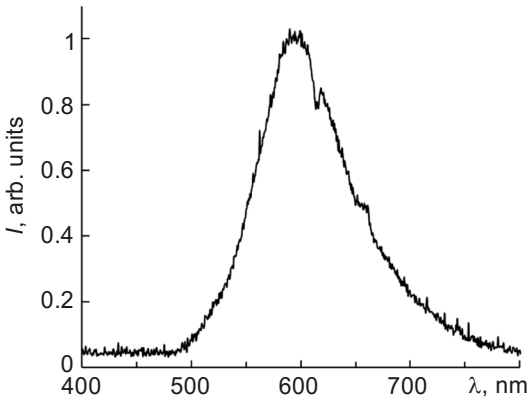

Fig. 2

Fig. 1. Transmission spectra of CVD-grown ZnSe (curve *1*) and Sm- (curve *2*), Te- (curve *3*) and Ga-alloyed (curve *4*) ZnSe crystals.

Fig. 2. Pulsed X-ray luminescence spectrum of ZnSe(Ga) crystal measured from its non-irradiated surface.

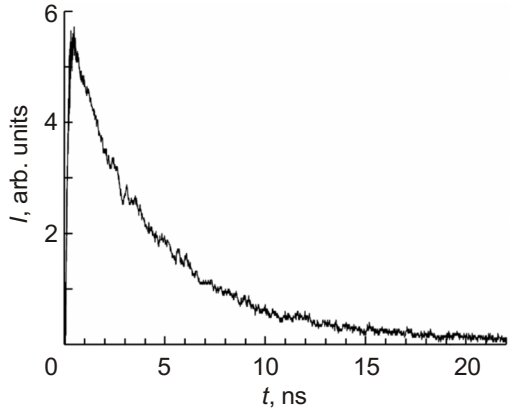

Fig. 3. Kinetics of pulsed X-ray luminescence of 600 nm wavelength in ZnSe(Ga) crystal.

For the Ga-alloyed crystal, the kinetics of the luminescence decay in this band is shown in Fig. 3 that describes it by the exponential function with the relaxation time of ~5 μs. For crystals alloyed by other elements, this kinetics

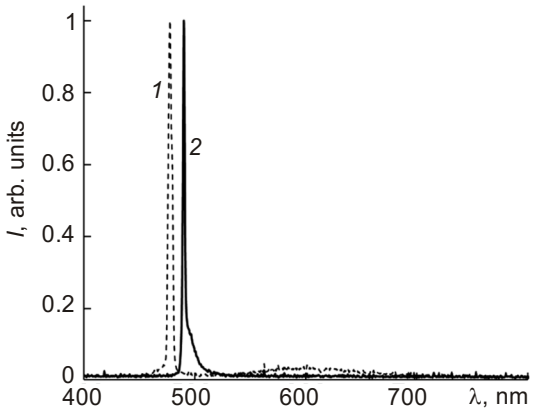

Fig. 4. Pulsed cathodoluminescence spectra of ZnSe(Ga) (curve *1*) and CVD-grown ZnSe (curve *2*) crystals measured at the ends at $H = 0.25$ J/cm^2.

shows a 4–7 μs change, while in the CVD-grown ZnSe crystal its intensity is at least two orders of magnitude less and is not recorded in the pulsed X-ray luminescence spectrum.

Information about the luminescence mechanism in a 600 nm wavelength region and the nature of the respective luminescence centers in ZnSe was given in [15]. Typically, the nature was associated with various compositions, which included intrinsic defects and impurities. In [15], it was shown that semiconductors of A_2B_6 (ZnS, ZnSe, CdS) group always contained oxygen as a background impurity, and its limit concentration could reach 10^{20} cm^3. Based on the experimental data, it was concluded [15] that the radiative-recombination centers responsible for the 600 nm band, were thermodynamically stable, non-mobile ternary complexes, that included zinc vacancy, interstitial zinc atom and oxygen in the lattice site ($V_{Zn}Zn_iO_{Se}$). Oxygen stabilized closely spaced intrinsic defects ($V_{Zn}Zn_i$), while alloying impurities, on the one hand, increased the concentration of intrinsic defects and on the other, increased the oxygen solubility in the ZnSe crystal lattice. According to Table 1, the 600 nm band appeared regardless of the type of the implanted impurity. The introduction of gallium in ZnSe crystal led to a drastic increase at ~600 nm luminescence, due to probably the high concentration of ternary complexes ($V_{Zn}Zn_iO_{Se}$).

In the point by point recording of pulsed cathodoluminescence spectra of the CVD-grown and the alloyed ZnSe crystals, the peak intensity at 490 and 477 nm, respectively, is observed at the moment of excitation at the energy density $H > 0.06$ J/cm^2. In the light sum per pulse recording of pulsed cathodoluminescence spectra of the alloyed ZnSe crystals, two spectral bands with maxima at ~477 and ~600 nm are observed. Their relative intensity depends on the energy density and the geometry of spectrum measurements. Figure 4 shows the pulsed cathodoluminescence spectra of CVD-grown and Ga-alloyed ZnSe crystals measured at their ends at $H = 0.25$ J/cm^2. The second band emerges at 600 nm in the ZnSe(Ga) crystal due to the light sum per pulse recording, *i.e.* $S = I_0 \cdot \tau$, where I_0 is the luminescence at the end of the pulse, τ is the time constant of luminescence decay. Since the light sum per pulse for the cathodoluminescence bands with maxima at about 490 and 600 nm are comparable, they are recorded in the spectrum simultaneously. The ratio between these band intensities depends on the concentration of the ternary complexes, e-beam energy density and geometry of spectrum measurements. For example, at $H \sim 0.25$ J/cm^2, in pulsed cathodoluminescence spectra measured at the end of the ZnSe(Ga) crystal, the 477 nm illumination predominates ($\alpha = 90°$ for excitation and registration geometry) (Fig. 4, curve *1*).

As can be seen from Fig. 5 (curve *2*), at $H \sim 0.15$ J/cm^2 and the same excitation and radiation conditions ($\alpha = 90°$), the relative intensity at 600 nm wavelength increases. When the cathodoluminescence spectrum of the ZnSe(Ga) crystal is measured on the non-irradiated surface ($H \sim 0.15$ J/cm^2), 600 nm wavelength predominates in this spectrum (curve *1*).

The analysis of pulsed cathodoluminescence spectra of the absorption edge of the ZnSe(Ga) crystal shows that when the e-beam incident angle changes relative to the normal surface of the crystal, a shift is observed for the absorption edge maximum. For example, at $\alpha = 45°$ geometry, the maximum is observed at 471 nm, but when

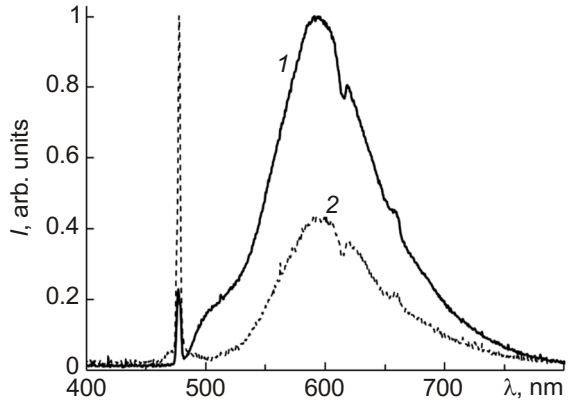

Fig. 5. Pulsed cathodoluminescence spectra measured at H = 0.15 J/cm^2 on the non-irradiated surface (curve *1*) and at the end (curve *2*) of ZnSe(Ga) crystal.

measuring at the crystal end or its non-irradiated surface, the cathodoluminescence spectrum shifts toward 477–478 nm wavelength region that is explained by reabsorption of the short-wave band edge during the radiation transfer in the crystal.

The explanation for the formation laws of the pulsed X-ray and cathodoluminescences of the alloyed ZnSe single crystals can be the following. At low levels of the crystal excitation corresponding to the X-ray radiation ($G \sim 10^{19}$–10^{20} cm^{-3}·s^{-1}), recombination of nonequilibrium charge carriers occurs mainly on defects and is accompanied by the 600 nm radiation, which is the main in the X-ray luminescence spectrum in light sum per pulse recording. During the e-beam irradiation of the crystal specimens, the excitation level reaches 10^{26}–10^{27} cm^{-3}·s^{-1}. With increasing excitation level, the intensity saturation occurs at ~600 nm luminescence due to the limit concentration of the luminescence centers, while the intrinsic edge self-radiation continues to increase. Thus, in the ZnSe(Ga) crystal, at the threshold energy density of the e-beam, the spontaneous luminescence (FWHM ~ 54 meV) transfers to the optically stimulated one, as evidenced by a drastic intensity increase in the absorption band edge at 477 nm and its narrowing (FWHM ~ 22 meV). Since the optically stimulated luminescence propagates in the direction normal to the e-beam incidence, the narrow line of 477 nm stimulated luminescence is observed in the spectrum when measuring pulsed cathodoluminescence at the crystal edge. In recording the cathodoluminescence spectrum on the non-irradiated crystal surface, 600 nm illumination predominates in the spectrum. At α = 45° geometry, two spectral bands of pulsed cathodoluminescence are observed, *viz*. the band edge and that one with maximum at ~600 nm.

It should be noted that the regularities identified for the formation of the pulsed cathodoluminescence spectrum for the ZnSe(Ga) crystal are observed to some extent for the CVD-grown ZnSe crystal also. The main difference is that the pure ZnSe crystal has no oxygen absorption band with maximum at ~600 nm. In addition, the absorption band edge (spontaneous and stimulated luminescence) shifts by ~15 nm to the long-wave region relative to the transmission spectrum edge. This is probably because the influence of intrinsic and impurity defects on the CVD-grown ZnSe crystal that requires special studies of technological factors affecting the luminescence properties of these crystals.

The obtained results show the following advantages of using alloyed and non-alloyed ZnSe crystals for the control of escaping electrons and X-ray radiation in tokamak devices. Unlike alkali-halide crystals of the CsI(Tl) type, in the CVD-grown ZnSe and ZnSe(Ga) crystals exposed to the e-beam irradiation, the generation of stimulated radiation is observed at 490 and 477 nm, respectively. This effect can be used for the e-beam recording without using the optical fiber in tokamak devices for crystal radiation transport from the camera to the photodetector outside. As is known, plasma heating and loss in high energy of electrons generate the X-ray radiation, which has a significantly higher penetrating power (at the same energy of photons and electrons) than e-beams. X-rays penetrating the quartz optical fiber cause their radiance and distort the radiation spectrum of the crystals, thereby complicating recording of escaping electrons. X-rays may also affect photodetectors.

Of particular interest for the diagnosis of escaping electrons and attendant X-ray radiation is the ZnSe(Ga) crystal having the absorption band with maximum at ~600 nm, allowing recording of escaping electrons and pulsed X-ray radiation both from the tokamak plasma and pulses of escaping electrons.

CONCLUSIONS

The CVD-grown ZnSe crystals and those alloyed by elements belonging to groups III and VI, can be used in e-beam and X-ray detectors owing to their high efficiency of energy conversion of the e-beam and X-ray radiation into luminescence. The CVD-grown and ZnSe(Ga) crystals are the most suitable for creating such detectors. In design of escaping electron detectors, we also propose to use a low threshold, high intensity and direction of the stimulated radiation. This should help to avoid the use of optical fiber for the radiation transfer from crystals to photodiode. It is not possible to register the Vavilov-Cherenkov radiation, whose short-wave region coincides with the transmission edge in these crystals. Therefore, ZnSe crystals are not suitable for developing Cherenkov detectors.

This work was financially supported by Grant No. 18-19-00184 from the Russian Science Foundation with the partial financial support from National Research Tomsk Polytechnic University in the framework of the Competitiveness Enhancement Program.

REFERENECES

1. M. C. C. Pereira, T. M. Filho, J. R. Berretta, and C. H. Mesquita, Mat. Sci. Appl., **9**, No. 2, 268 (2018).
2. E. I. Lipatov, A. G. Burachenko, S. M. Avdeev, *et al*., Russ. Phys. J., **61**, No. 3, 469–483 (2018).
3. B. Pourshahab, M. R. Abdi, A. Sadighzadeh, and C. Rasouli, Phys. Plasmas, **23**, 072501 (2016).
4. R. J. Zhou, L. Q. Hu, Y. Zhang, *et al*., Nucl. Fusion, **57**, No. 11, 114002 (2017).
5. M. Rubel, S. Brezinsek, J. W. Coenen, *et al*., Matter Radiat. at Extremes, **2**, No. 3, 87 (2017).
6. L. Jakubowski, M. J. Sadowski, and J. Zebrowski, Rev. Sci. Instrum., **81**, No. 1, 013504 (2010).
7. F. Bagnato, A. Romano, P. Buratti, *et al*., Plasma Phys. Contr. Fusion, **60**, No. 11, 115010 (2018).
8. D. A. Sorokin, A. G. Burachenko, D. V. Beloplotov, *et al*., J. Appl. Phys., **122**, No. 15, 154902 (2017).
9. A. G. Burachenko, V. F. Tarasenko, D. V. Beloplotov, and E. Kh. Baksht, Russ. Phys. J., **60**, No. 9, 1533−1537 (2018).
10. V. F. Tarasenko, E. Kh. Baksht, D. V. Beloplotov, *et al*., Russ. Phys. J., **62**, No. 7, 1181–1190 (2019).
11. T. Zhao, M. Hu, R. Zhong, *et al*., Appl. Phys. Lett., **110**, No. 23, 231102 (2017).
12. V. F. Tarasenko, M. I. Lomaev, D. A. Sorokin, and D. V. Beloplotov, Russ. Phys. J., **61**, No. 7, 1361–1362 (2018).
13. K. V. Berezhnoy, A. S. Nasibov, A. G. Reutova, *et al*., Opt. Mem. Neural Networks, **18,** No. 4, 285 (2009).
14. V. I. Oleshko, E. Kh. Baksht, A. G. Burachenko, and V. F. Tarasenko, Tech. Phys., **62**, No. 2, 299 (2017).
15. N. K. Morozova, I. A. Karetnikov, and E. M. Gavrishchuk, Inorg. Mater., **35**, No. 8, 775–779 (1999).